Jordanian Journal of Engineering and Chemical Industries

Print ISSN: 2616 - 9584 Online ISSN: 2617 - 720X

Corrosion Susceptibility of Blued Steel Reinforcement in Concrete by Electrochemical Impedance Spectroscopy

Sami Masadeh

Materials Engineering Department, Al-Balqa Applied University, Al-Salt, P.O. Box 206, 19117, Jordan.

Abstract

The main aim of this study is to quantify the rate of corrosion in reinforced steel bars embedded within concrete structures exposed to a simulated high-chloride marine environment. This involved selecting specific frequencies that corresponded to the solution resistance and charge transfer resistance, enabling faster measurements. A total of five cement mortar specimens were meticulously prepared for the investigation. The study focused on assessing the impact of variations in bluing temperature on corrosion minimization. Bluing was carried out at 450, 550, 650, and 750ºC, and then immersing the specimens in a 3 wt.% NaCl solution for 21 days. Frequent tests, just after immersion, 7,14-, and 21-days immersions. Measurements through alternative current (AC) impedance were conducted across a frequency spectrum ranging from 100kHz to 10MHz. The results showed a significant decrease in the corrosion rate for specimens blued at 750, which was attributed to the development of thicker protective layers on the rebar. Higher corrosion rates were observed for bluing at lower temperatures.

Paper type: Research paper

Keywords: Steel reinforcement, concrete, electrochemical impedance spectroscopy, bluing.

Citation: Masdeh, S. "Corrosion Susceptibility of Blued Steel Reinforcement in Concrete by Electrochemical Impedance Spectroscopy", Jordanian Journal of Engineering and Chemical Industries, Vol. 6, No.3, pp: 66-71 (2023).

Introduction

Steel reinforcement corrosion is one of the primary factors causing concrete deterioration (Sohail, *et al.*, *2020*). This deterioration can lead to potentially hazardous issues (Dong, *et al.*, *2011*). Several factors influence and expedite the corrosion of steel in concrete, with chlorides primarily originating from marine or deicing salts and high humidity being the most significant contributors (Lu, *et al*., 2019; Austin *et al*., 2004; Chang *et al*., 2022; Cao, *et al.*, 2019). Numerous methods are available for protecting steel in concrete, including cathodic protection, the use of inhibitors, and proper steel surface coatings (Masadeh, 2015; Masadeh, 2013; Masadeh, 2005). Monitoring the corrosion of steel in concrete can be achieved through electrochemical techniques (Masadeh, 2005; Jeong, 2015), such as Electrochemical Impedance Spectroscopy, polarization methods, and electrochemical noise. These electrochemical tests are cost-effective, swift, and yield reliable results while measuring the severity of steel corrosion. Laboratory tests may yield less accurate results compared to real-world field conditions (Kim, *et al*., 2002). Polarization resistance, along with corrosion current density, is related both theoretically and experimentally. Corrosion resistance is highly valuable for calculating corrosion rates, and both AC and DC methods can be employed for this purpose. AC impedance analysis involves extrapolating impedance values to frequencies (Faustin, *et al.*. 2015). Electrochemical impedance spectroscopy (EIS) can provide insights into various electrochemical mechanisms, including the role of electrode processes and their contributions to these mechanisms (Nishikata, 2014). EIS employs AC current and assesses spectrochemical methods that depend on the nature of electrolytic activities. It can detect the corrosion susceptibility of steel in concrete. At lower frequencies, the determination of charge transfer becomes possible (Ryl, 2008) and each frequency range can predict the reactions occurring at the metal/concrete interface (Langford and Broomfield, 1987). At higher frequencies, the components of the solution may separate, allowing for correction in the dynamic voltage (IR) drop. Consequently, the corrosion mechanism can be examined, and the causes of corrosion, based on frequency and speed, can be identified. Over time, oxides form on metal surfaces, affecting the rate and potential for corrosion. In conventional EIS experiments, the corrosion potential or fixed voltage is established at the outset to measure the constantly changing surface corrosion rate.

* Corresponding author: E-mail: masadeh@bau.edu.jo ORCID: https://orcid.org/0000-0002-1932-8810

Received on October 31, 2023. Accepted on November 28, 2023.

Jordanian Journal of Engineering and Chemical Industries (JJECI), Vol.6, No.3, 2023, pp: 66-71. Revised: November 30, 2023.

Dynamic EIS measures the rate of oxide corrosion on the metal surface with a separate reference electrode and varying potential, focusing on the evolution of corrosion behaviour over time (Jing, *et al.*, 2014).

The objective of this study is to determine whether applying bluing to steel reinforcement at different temperatures can reduce the rate of steel corrosion in concrete. The study evaluates the parameters affecting the non-uniformity of current distribution and the IR drop on the surface of the reinforced bar (rebar). Mortar specimens with embedded rebars are exposed to repeated cycles of immersion in a 3 wt.% sodium chloride solution and subsequent drying at room temperature to replicate a maritime environment. By utilizing two selected frequencies for high-speed monitoring, the corrosion rate of the rebars is tracked.

1 Materials and Methods

1.1 EIS Circuit for steel in concrete

The Electrochemical Impedance Spectroscopy (EIS) technique employs the frequency domain to represent the interface of the rebar embedded in concrete as an equivalent electric circuit consisting of resistance, inductance, and capacitance (Masadeh, 2013). This study employs the EIS equivalent circuit model, which comprises the Warburg impedance (W), constant phase element, solution resistance, and charge transfer resistance (as illustrated in **Figure 1**). In this context, R_s represents the electromotive force generated within the electrolyte solution present in the cement void. The resistance of the corrosion mechanism to charge transfer is denoted by the abbreviation R_c, The electric double layer capacity C_{dl}, pertains to the double layer capacity at the interface of the cement mortar and rebar, while W refers to the electrical double-layer capacity.

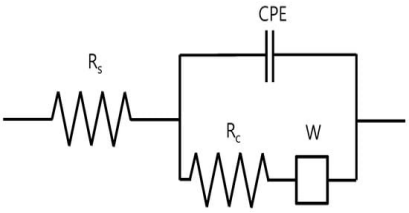

Fig. 1 A reinforced steel in concrete equivalent electrochemical impedance spectroscopy (EIS) model.

The overall impedance Z, is given by equation 1, where j is a complex number given by the frequency response analyser and ω is the frequency, represented as:

$$Z=R_S+(R_c/1+j\omega C_{dl}R_c) \quad (1)$$

The inverse of C_{dl0} which is the capacitor impedance can determine R_s, where R_s+R_c can be determined at low frequency. The difference between high and low frequencies can determine R_p, the polarization resistance (Langford, 1987). However, the Stern-Geary equation was used to calculate the corrosion current density using polarization resistance.

1.2 Specimen preparation

Table 1 Bluing temperatures of steel rebars.

Sample	Bluing Temperature, °C
1	No Blue
2	450
3	550
4	650
5	750

Steel reinforcements with a diameter of 10mm and a length of 80mm were cut from steel bars. Following a pickling treatment, all steel reinforcements were subjected to bluing by heating and then quenching them in engine oil. The bluing process was conducted at different temperatures, specifically 450, 550, 650, and 750°C, as detailed in **Table 1**. As illustrated in **Figure 2**, concrete specimens were configured with a central steel reinforcement bar measuring 10mm in diameter and 80mm in length. Each rebar underwent bluing at different temperatures, with the sample numbers and corresponding bluing temperatures outlined in Table 1. The steel rebars were centrally positioned within rectangular molds with dimensions of 50x50x100 mm, as depicted in the schematic configuration in Fig. 2. To ensure a consistent exposed area to concrete for each rebar (10cm²), epoxy paint was applied to coat the rebars, maintaining the same exposed surface area across all samples. The cement mix was prepared using Portland cement with a water-cement ratio of 0.5 and a cement-sand ratio.

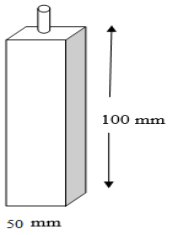

Fig. 2 Configuration of reinforced concrete specimens.

1.3 Electrochemical impedance and potential measurements:

The electrochemical impedance measurements of the reinforced concrete samples were conducted using a double-electrode system. The test samples were immersed in a 3.5% NaCl solution, which was prepared using distilled water and laboratory-grade sodium chloride. The electrochemical impedance tests were carried out during various immersion periods.

For the EIS tests, specimens were subjected to analysis using the Princeton A273 potentiostat instrument equipped with a Frequency Response Analyzer (FRA). The potential of the reinforcements was measured using a calomel-saturated electrode (CSE). The electrochemical impedance measurements utilized a frequency range from 100kHz to 10MHz, with five frequencies per decade and an AC amplitude of ±10mV. The current required to induce this potential disturbance was measured, along with the shift in the phase of the current and potential characteristics. An applied DC voltage of ±10mV, was used. The charge transfer resistance R_c and solution resistance R_s were calculated through regression analysis. For the purpose of comparison, an unblued reinforced concrete specimen was tested using the same solution and EIS configuration. The experimental setup is depicted in **Figure 3**.

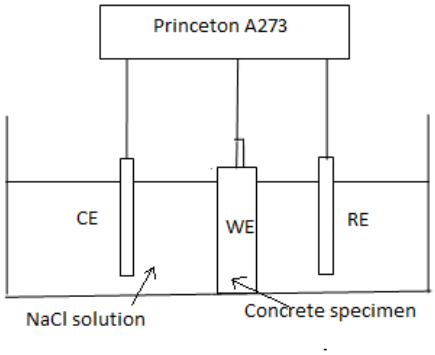

Fig. 3 EIS experimental setup using Princeton A273.

2 Results and Discussion

Figure 4 represents Nyquist plots for unblued steel over the entire test period of twenty-one days during different immersion periods. **Figures 5-8** represent Nyquist plots for blued steel at various temperatures. As illustrated in Fig. 4, all Nyquist plots consistently display a single depressed capacitive arc, reflecting the measured impedance values for all specimens tested in a 3.5% NaCl solution immediately after immersion and at seven, fifteen days, and twenty days. Above the 10kHz frequency range, the tail of the arc is well-defined, while at lower frequencies, the arc appears larger and incomplete, indicating the potential for corrosion.

Electrochemical parameters, including solution resistance R_s, charge transfer resistance R_c, and polarization resistance R_p are presented in **Table 2**, as provided by the EIS software accompanying the instrument. These values are in alignment with the changes in Rc values corresponding to the bluing temperature. R_p increases with higher bluing temperatures, suggesting lower expected corrosion rates for higher bluing temperatures. In several investigations, it has been noted that the corrosion of steel bars contributes to a rise in the capacitive reactance within the cement paste that reinforces the steel bars. This elevated capacitive reactance impedes electron migration (Duffoa, *et al.*, 2009, Qiao, *et al.*, 2012, Liu, *et al.*, 2019, Zhang, *et al.*, 2018). Consequently, the cement paste, which is reinforced with more severely corroded steel bars, exhibits greater fluctuations in electrical resistance when subjected to direct current in the specimens. It's worth noting that the values of solution resistance were observed to be within approximately the same range, while charge transfer resistance values notably increased for specimens blued at 750°C. In contrast, slight changes were observed for specimens blued at 450, 550, and 650°C. This observation indicates a reduced susceptibility to corrosion in the latter cases.

Table 2 Electrochemical impedance parameters as took from instrument fitting software.

	No blue	450°C	550°C	650°C	750°C
R_s ((kΩcm^2)	3.6	3.5	3.4	3.7	3.6
R_p ((kΩcm^2)	19	70	78	91	127
R_c ((kΩcm^2)	227	967	2139	4691	11282

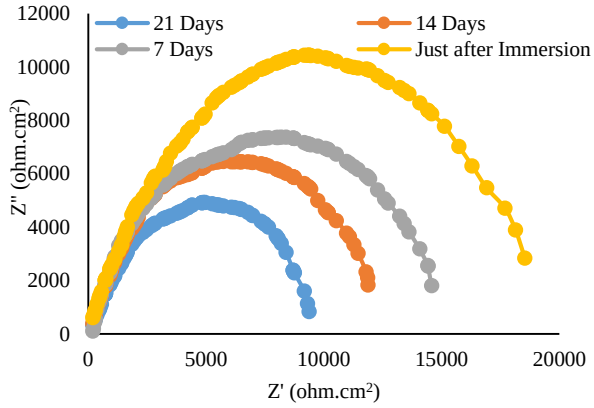

Fig. 4 Nyquist plot of non-blued steel reinforcement at different immersion periods.

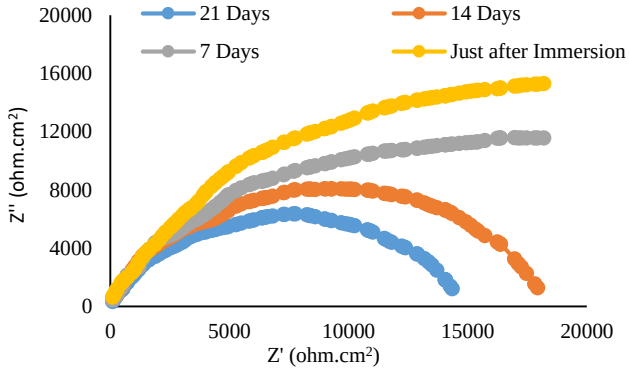

Fig. 5 Nyquist plot of blued steel at 450°C at different immersion periods showing Warburg impedance.

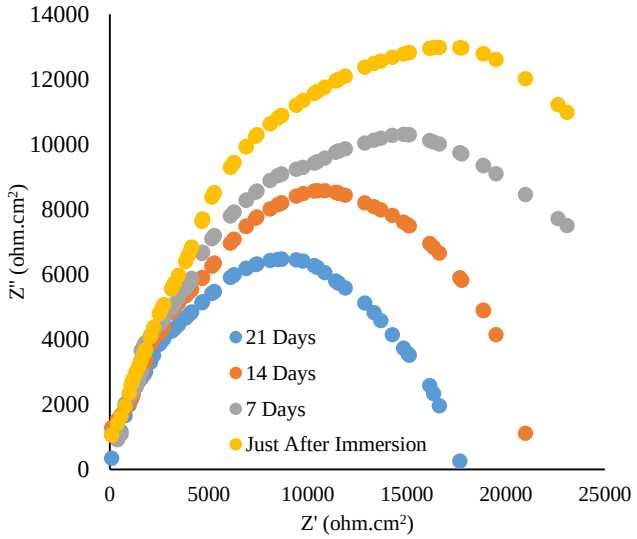

Fig. 6 Nyquist plot of blued steel at 550°C at different immersion periods showing Warburg impedance.

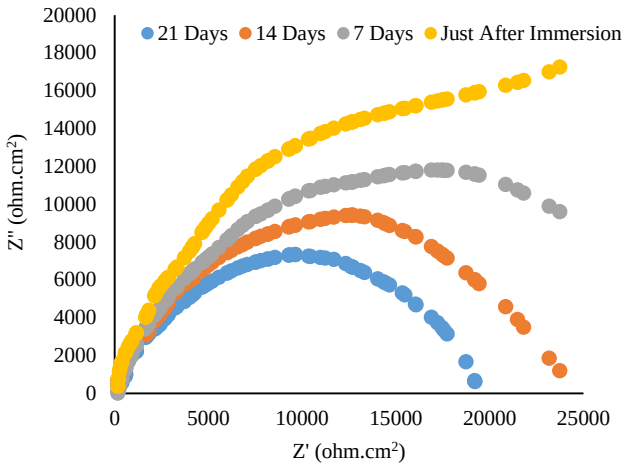

Fig. 7 Nyquist plot of blued steel at 650°C at different immersion periods.

Notably, as the bluing temperature increases, the radius of this capacitive arc for tests conducted immediately after immersion proportionally expands. This observation suggests that the bluing temperature does not alter the fundamental corrosion mechanism; rather, it reduces corrosion by forming a thicker protective film on the steel's surface. With increasing immersion time, a depression in the semicircle is observed for non-blued steel, while for blued steel at all temperatures, the impedance spectrum comprises two sections connected by a straight line. The diameter of the semicircle represents the charge transfer resistance, whereas the straight line indicates the dominant Warburg impedance at low frequencies due to diffusion (Jing, 2014). The equivalent circuit of blued specimens, with Warburg impedance, is illustrated in Fig. 2. As

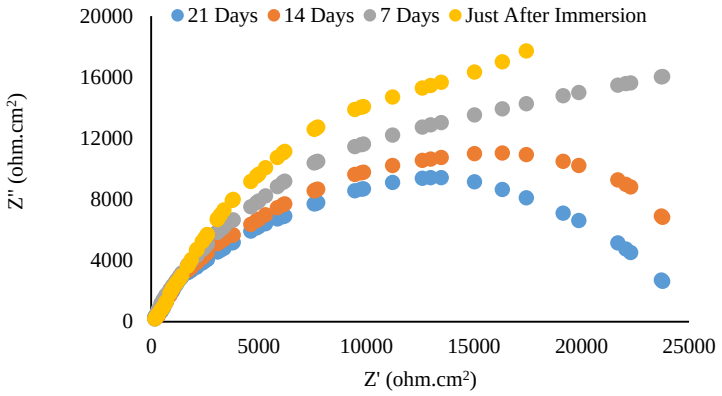

Fig. 8 Nyquist plot of blued steel at 750°C at different immersion periods.

observed in Figures 4 to 8, the polarization resistance increases for blued specimens at higher temperatures, indicating a lower corrosion rate since the corrosion rate is inversely proportional to polarization resistance. The influence of bluing temperature on corrosion protection may be attributed to the type of layer formed on the steel reinforcement surface. It is expected that at higher temperatures, a Hematite (Fe_2O_3) layer is formed, whereas at lower temperatures Magnetite (Fe_3O_4) is formed. Another factor to consider is that the layer thickness increases as the bluing temperature rises. The oil quenching temperature can impact the type of scale that forms on the steel surface during the quenching process. The temperature at which the steel is quenched can influence the oxidation reactions occurring on the When steel is quenched at lower temperatures, there is less energy available for oxidation reactions. The scale formed at lower quenching temperatures is typically thinner and may consist mainly of magnetite (Fe_3O_4) and wüstite (FeO). These are iron oxide phases that can form under reducing (low oxygen) conditions. The scale at lower temperatures may have a darker colour, often appearing as black or dark grey, due to the presence of these iron oxide phases.

When quenching occurs at higher temperatures provides more energy for oxidation reactions with atmospheric oxygen. The scale formed at higher quenching temperatures is usually thicker and may contain a greater proportion of hematite (Fe_2O_3), another iron oxide phase. The scale at higher temperatures may exhibit a more varied colouration, including reddish-brown or bluish hues, due to the presence of hematite and other iron oxide compounds. At intermediate quenching temperatures, the scale composition and appearance can vary, depending on the specific conditions. The scale may consist of a combination of iron oxide phases, such as magnetite, wüstite, and hematite, resulting in a mixed-color appearance.

It should be emphasized that the precise temperature ranges for lower, intermediate, and higher quenching temperatures can fluctuate, dependent on variables like steel composition, the choice of quenching oil, and various other considerations. Additionally, the surrounding environment during the quenching process, whether it's conducted in air, under inert gas, or otherwise, can exert an influence on oxidation reactions. In the initial phase of the EIS test, the rebar/mortar is represented using a simplified equivalent circuit. As the immersion period progresses, the entry of chloride ions leads to a reduction in the charge transfer resistance. Simultaneously, the appearance of the Warburg impedance, signifying oxygen diffusion within the mortar, is detected within the lower frequency range, for higher bluing temperatures, both the corrosion rate and the R_s of the rebars were notably observed to escalate. The R_s value was also higher for the non-blued steel, which can be attributed to thinner electrolyte layers and an increased corrosion rate of the rebar. This elevated corrosion rate implies the formation of oxide layers during the immersion. While monitoring the corrosion rate through AC impedance, precise measurement of the polarization resistance was achieved by compensating for the IR drop, taking into account the specimen's dry condition and the quantity of corrosion products identified on the rebar's surface.

Conclusions

In the initial phase of all specimens can be characterized by a basic equivalent circuit. As time passes, the penetration of chloride ions leads to a reduction in charge transfer resistance. Simultaneously, the appearance of the Warbug impedance, signifying oxygen diffusion within the mortar, becomes noticeable at lower frequencies. For non-blued and specimens blued at 450ºC, there was a notable rapid increase in both the corrosion rate and the resistance R_s of the rebars. Bluing at 450ºC, and at 550ºC, the R_s value was seen to elevate, primarily due to the presence of thinner electrolyte layers and an accelerated corrosion rate of the rebar. While monitoring the corrosion rate through AC impedance, precise measurement of the polarization resistance was achieved by adjusting for the IR drop, taking into account the specimen's bluing temperature and the quantity of corrosion products present on the rebar's surface. The given polarization resistance value, incorporating R_s, differed from the polarization resistance value without Rs correction, owing to factors such as the drying condition, the presence of a rust layer, and the electrode spacing. Bluing at 750ºC showed good protection against corrosion in NaCl solution, due to thicker and different layer formed at steel surface. Bluing at 550, and 650ºC, had a noticeable diffusion, can lead to corrosion at longer times.

Nomenclature

C_{dl}	=double layer capacity at the interface between cement mortar and rebar	[μF/cm^2]
C_{dl0}	=C_{dl} approaches zero	[μF/cm^2]
IR	=current by resistance	[volts]
J=	=complex number that is determined by the frequency response analyzer	[-]
R_c	=charge transfer resistance	[S/m]
R_c	=the resistance of the charge transfer involved in the corrosion mechanism.	[S/m]
R_S	=solution resistance	[S/m]
ω	=frequency	[Hz]
Z	=total impedance	[Ohm.cm^2]

References

Austin, S. A., Lyons, R., and M., Ing "Electrochemical behavior of steel reinforced concrete during accelerated corrosion testing", *Corrosion*, **60**, 203–212, (2004).

Cao, M., Liu, L., Yu, Z., Fan, L., Li, Y., and F., Wang "Electrochemical corrosion behavior of 2A02 Al alloy under an accelerated simulation marine atmospheric environment", *J. Mater. Sci. Technol.*, **35**, 651–659 (2019).

Chang, C. W, Tsai, C. A., and Y., and Y. C., Shiau "Inspection of steel bars corrosion in reinforced concrete structures by nondestructive ground penetrating radar", *Appl. Sci.*, **12**, 5567, (2022).

Dong, S. G., Lin, C. J., Hu, R. G., Li, L. Q., and R. G., Du "Effective monitoring of corrosion in reinforcing steel in concrete constructions by a multifunctional sensor", *Electrochim. Acta*, **56**, 1881–1888, (2011).

Duffoa, G., Farinab, S., and C., Giordano "Characterization of solid embeddable reference electrodes for corrosion monitoring in reinforced concrete structures" *Electrochim. Acta*, **54**, 1010–1020, (2009).

Jeong, J. A. "Consideration on the Risk of Corrosion Assessment in Reinforced Concrete Structure by Corrosion Potential Criterion", *Corros. Sci. Technol.*, **14**, 147–152, (2015).

Jing, X., Cao, X., Wang, L., Lan, T., Li, Y., and G., Xie, "DNA-AuNPs based signal amplification for highly sensitive detection of DNA methylation, methyltransferase activity and inhibitor screening. Biosens", *Bioelectron*, **58**, 40–47, (2014).

Kim, J.K., Nishikata, A., and T., Tsuru "Impedance Characteristics of Reinforcing Steel in Mortar and Corrosion Monitoring", *Zairyo-to-Kankyo*, **51**, 57–67, (2002).

Liu, M., Tan, H., and X., He "Effects of nano-SiO2 on early strength and microstructure of steam-cured high volume fly ash cement system", *Constr. Build. Mater.*, **194**, 350–359, (2019).

Lu, S., and H. J., Ba "Corrosion sensor for monitoring the service condition of chloride-contaminated cement mortar", *Sensors*, **10**, 4145–4158, (2010).

Faustin, M. A., Maciuk, P. Salvin, C. Roos and M. Lebrini, *Corrosion Sci.*, **92**, 287-300, (2015).

Masadeh, S., "Performance of Galvanized Steel Reinforcement In Concrete In Sea And Dead Sea Water", *J. of Mater. Sci. and Chem. Eng.*, **3**, 46-53, (2015).

Masadeh, S., "The Effect of Added Carbon Black to Concrete Mix On Corrosion Of Steel In Concrete", *J. of Minerals and Mater. Characterization and Eng.*, **9**, 271-376, (2015).

Masadeh, S., "The Influence of Added Inhibitors on Corrosion Of Steel In Concrete Exposed To Chloride Containing Solutions", *Adv. In Mater. Sci.*, **1**3, 5-11, (2013).

Masadeh, S., "Electrochemical Impedance Spectroscopy Of Epoxy-Coated Steel Exposed To Dead Sea Water", *J. of Minerals and Mater. Characterization and Eng.*, **4**, 75-84, (2005).

Nishikata, A., Zhu, Q., and E Tada "Long-term monitoring of atmospheric corrosion at weathering steel bridges by an electrochemical impedance method", *Corros. Sci.*, **87**, 80–88, (2014).

Langford, P, and J., Broomfield "Monitoring the corrosion of reinforcing steel", *Constr. Repair*, **1**, 32–36, (1987).

Qiao, G., Hong, Y., Song, G., Li, H., and J., Ou "Electrochemical characterization of the solid-state reference electrode based on NiFe2O4 film for the corrosion monitoring of RC structures", *Sens. Actuators B:Chem.*, **168**, 172–177, (2012).

Ryl, J., and K., Darowicki "Impedance Monitoring of Carbon Steel Cavitation Erosion under the Influence of Corrosive Factors", *J. Electrochem. Soc.*, **155**, 44–49, (2008).

Sohail, M. G., Kahraman, R., Alnuaimi, N. A., Gencturk, B., Alnahhal, W., Dawood, M., and A., Belarbi, "Electrochemical behavior of mild and corrosion resistant concrete reinforcing steel", *Constr. Build. Mater.*,**232**, 117205, (2020).

Zhang, B., Tan, H., Shen, W., Xu, G., Ma, B., and X., Ji "Nano-silica and silica fume modified cement mortar used as Surface Protection Material to enhance the impermeability", *Cem. Concr. Compos.*, **92**, 7–17, (2018).